Article

Decomposition of Gaseous Styrene Using Photocatalyst and Ozone Treatment

Kengo Hamada *, Tsuyoshi Ochiai, Daisuke Aoki, Yasuhisa Akutsu and Yasuo Hirabayashi

Kawasaki Technical Support Department, Local Independent Administrative Agency Kanagawa Institute of Industrial Science and Technology (KISTEC), Ground Floor East Wing, Innovation Center Building, KSP, 3-2-1 Sakado, Takatsu-ku, Kawasaki-shi 213-0012, Japan; pg-ochiai@kistec.jp (T.O.); d-aoki@kistec.jp (D.A.); akutsu@kistec.jp (Y.A.); hirabaya@kistec.jp (Y.H.)
* Correspondence: k-hamada@kistec.jp; Tel.: +81-44-819-2105

Abstract: Because photocatalysis has strong oxidation abilities in redox systems, it has been applied to indoor air purification. However, intermediate products are produced during the photocatalytic oxidative decomposition of aromatic compounds with benzene rings. Therefore, it is essential to improve decomposition performance and evaluate the intermediate products produced for practical applications. Herein, we describe the decomposition performance of ozone, photocatalyst, and their combination, under the target gas of styrene. Using a one-pass mini reactor, decomposition performance was evaluated by analyzing the output gas in the reactor and observing the styrene removal, the amount of carbon dioxide produced, and the composition of a small amount of intermediate products. The combination of ozone and photocatalyst showed the most significant performance, completely decomposing in the photocatalyst and removing odor components in ozone. Moreover, we demonstrated that decomposition performance could be evaluated by observing slight amounts of intermediate products in the exhaust gas. We believe that this research provides insights into the practical application of photocatalysis and ozone oxidation technologies in air purifiers and their performance management, with particular emphasis on the decomposition of odor compounds.

Keywords: photocatalyst; TiO$_2$; ozone; AOPs; styrene; intermediates; decomposition; air purification; air purifier

1. Introduction

Photocatalysts have demonstrated strong oxidation abilities in redox systems since Fujishima et al. first reported them in the 1970s [1–3]. A leading photocatalyst is titanium dioxide (TiO$_2$), and its strong oxidation ability and superhydrophilicity are accelerating its application in the fields of antibacterial, antiviral, antifogging, and environmental purification [4–7]. Titanium dioxide is chemically stable and resourceful; moreover, its optical properties make it widely used in sunscreens, white paints, food products, and other applications [8]. TiO$_2$ photocatalyst is based on anatase structure with nanoparticles, which has a wider band gap and stronger oxidative abilities than other crystalline structures [9,10]. Furthermore, its oxidation abilities are caused by reactive oxygen species on the surface of the photocatalyst, which are generated from the charge separation resulting from the absorption of ultraviolet light [3]. Several studies have investigated reactive oxygen species generated by photocatalysts that can decompose and remove pollutants in the environment for water and air purification [11–13]. In recent years, owing to the severity and diversification of air pollution, such as third-hand smoking and COVID-19, indoor air purification has been attracting attention, and the application of photocatalysts to air purifier filters has been promoted [14–17].

The JIS and ISO standard test methods are generally used to evaluate the performance of photocatalysts for air purification [18–20]. In this method, photocatalysts are evaluated by observing the amount of volatile organic compounds (VOCs) removed and the amount

of carbon dioxide produced by their decomposition [20]. However, it is known that intermediate products are produced during the photocatalytic oxidative decomposition of compounds with benzene rings with large molecular weights [21,22]. Therefore, to effectively apply photocatalysts for filters and air purifiers, it is important to evaluate the intermediate products in the exhausted gas as well as the JIS and ISO standard test.

On the other hand, ozone and ozone-based advanced oxidation processes (AOPs) are also known to have strong oxidation abilities [23–25]. It has been reported that organic substances can be decomposed by ozone or several active oxidative species produced by ozone irradiation with ultraviolet light [26–29]. Moreover, for air purification, several studies have reported combined photocatalyst and ozone treatment to improve decomposition performance and to avoid deactivation of the photocatalyst [30,31]. However, few studies have focused on the fundamental understanding of the decomposition of volatile organic compounds and the generation of intermediate products and standard methods of analysis for these technologies.

In this study, we focused on the decomposition performance and behavior of ozone, photocatalysts, and their combination by observing the intermediate products desorbed from photocatalysts, as well as the conventional evaluation method of measuring the amount of odorants removed and the amount of carbon dioxide produced. A small amount of intermediate products produced in each reaction was observed by gas chromatography-mass spectrometry (GC-MS) analysis, using the solvent extraction method. The results showed that the decomposition performance of odor components was improved, and the intermediate products and ozone in the exhaust gas could be suppressed by combining the photocatalyst and ozone, compared to the single treatment. This study may contribute to the development and quality control of air purifier products with the application of photocatalysts and ozone.

2. Results

Figure 1 shows a typical data set of styrene removal by reaction with each ozone concentration. After ozone mixing started, the rate of styrene concentration at the outlet decreased rapidly between 0.6 and 0.2 of the initial concentration, depending on the mixed ozone concentrations. The styrene concentration became constant within 15 min after the start (Figure 1a). The decrease in styrene concentration was independent of UV irradiation and remained constant. In addition, the production of carbon dioxide due to the reaction of styrene with ozone was not observed (Figure 1b). The gaseous components present at the reactor outlet were evaluated by gas chromatography-mass spectrometry (GC-MS). Figure 2 shows gas chromatograms of gas components at the reactor outlet by the activated carbon tube solvent extraction method (red: with ozone and UV irradiation, blue: with ozone only). The chromatogram showed peaks for benzene (23.8 min), styrene (35.2 min), benzaldehyde (38.8 min), styrene oxide (41.8 min), benzoic acid (45.6 min), and components unrecognizable by similarity measures (28.9 min). Moreover, their chromatograms did not change with or without UV irradiation, and the positions and intensity ratios of each peak were of the same value.

The ozone gas concentration at the reactor outlet was measured using the gas-detection tube method. Figure 3 shows the residual concentration and residual rate of ozone at the reactor outlet for each condition. For all ozone concentrations, ozone was not consumed without the presence of styrene in the reactor (black bars). When styrene was present in the reactor, ozone was consumed, and the concentration decreased compared to no reaction (red and blue bars). When UV irradiation was applied, the ozone concentration tended to be lower than that without irradiation. In addition, as the injected ozone concentration increased, the residual ozone rate increased.

Figure 4 shows a typical data set of styrene removal (red) and CO_2 generation (green) for each condition. The material balance data (Figure 4d) under each condition were estimated from these results. In the reaction of photocatalysis and UV irradiation, the styrene concentration was reduced to approximately half, and carbon dioxide was simultaneously

produced at approximately 90% of the ideal value (Figure 4a). In the reaction of ozone and UV irradiation, the styrene concentration decreased to approximately 30% of the initial concentration, but no carbon dioxide was produced (Figure 4b). In the reaction combining photocatalyst and ozone, the styrene concentration was reduced to approximately 30% of the initial concentration, and carbon dioxide was produced at the same time (Figure 4c). The amount of styrene removal was the same as that in reaction (b), and the production of carbon dioxide was the same as in reaction (a).

Figure 4 shows a typical data set of styrene removal (red) and CO_2 generation (green) for each condition. The material balance data (Figure 4d) under each condition were estimated from these results. In the reaction of photocatalysis and UV irradiation, the styrene concentration was reduced to approximately half, and carbon dioxide was simultaneously produced at approximately 90% of the ideal value (Figure 4a). In the reaction of ozone and UV irradiation, the styrene concentration decreased to approximately 30% of the initial concentration, but no carbon dioxide was produced (Figure 4b). In the reaction combining photocatalyst and ozone, the styrene concentration was reduced to approximately 30% of the initial concentration, and carbon dioxide was produced at the same time (Figure 4c). The amount of styrene removal was the same as that in reaction (b), and the production of carbon dioxide was the same as in reaction (a).
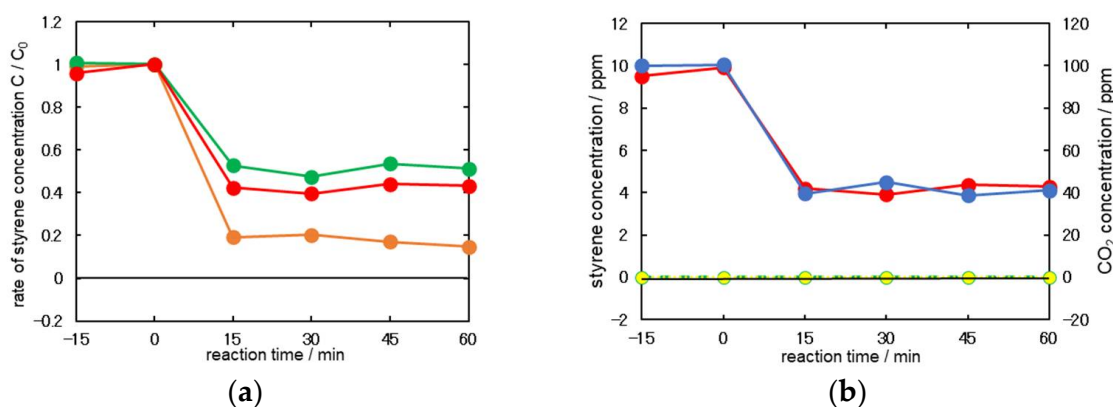

Figure 1. (**a**) Typical data set of styrene removal by reaction with each ozone concentration (green, red, and orange indicate 7 ppm, 12 ppm, and 22 ppm, respectively). (**b**) Typical data set of styrene removal (red, blue) and CO_2 generation (green, yellow) by reaction with ozone (red, green: with UV irradiation, blue, yellow: without UV irradiation).
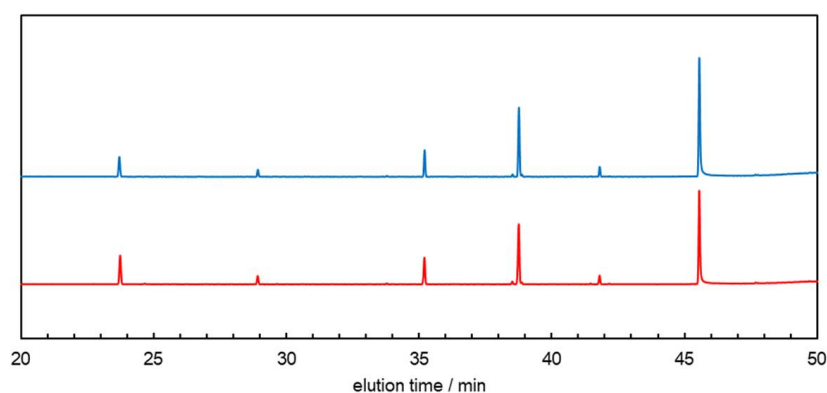

Figure 2. Gas chromatograms of gas components at reactor outlet by activated carbon tube–solvent extraction method (red: with ozone and UV irradiation, blue: with ozone only).
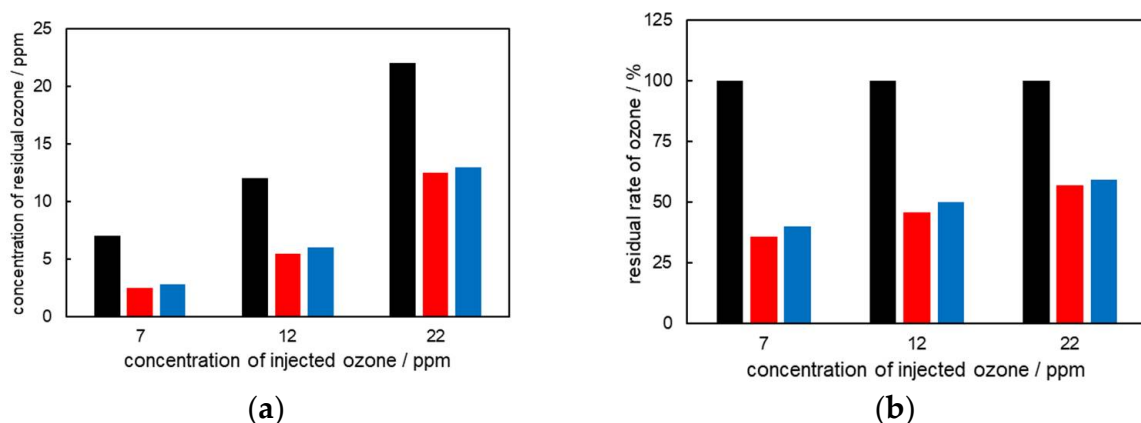
(**a**)

(**b**)

Figure 3. (**a**) Residual ozone concentration, (**b**) residual rate of ozone under each condition (black: without reaction, red: with UV irradiation, blue: without UV irradiation).
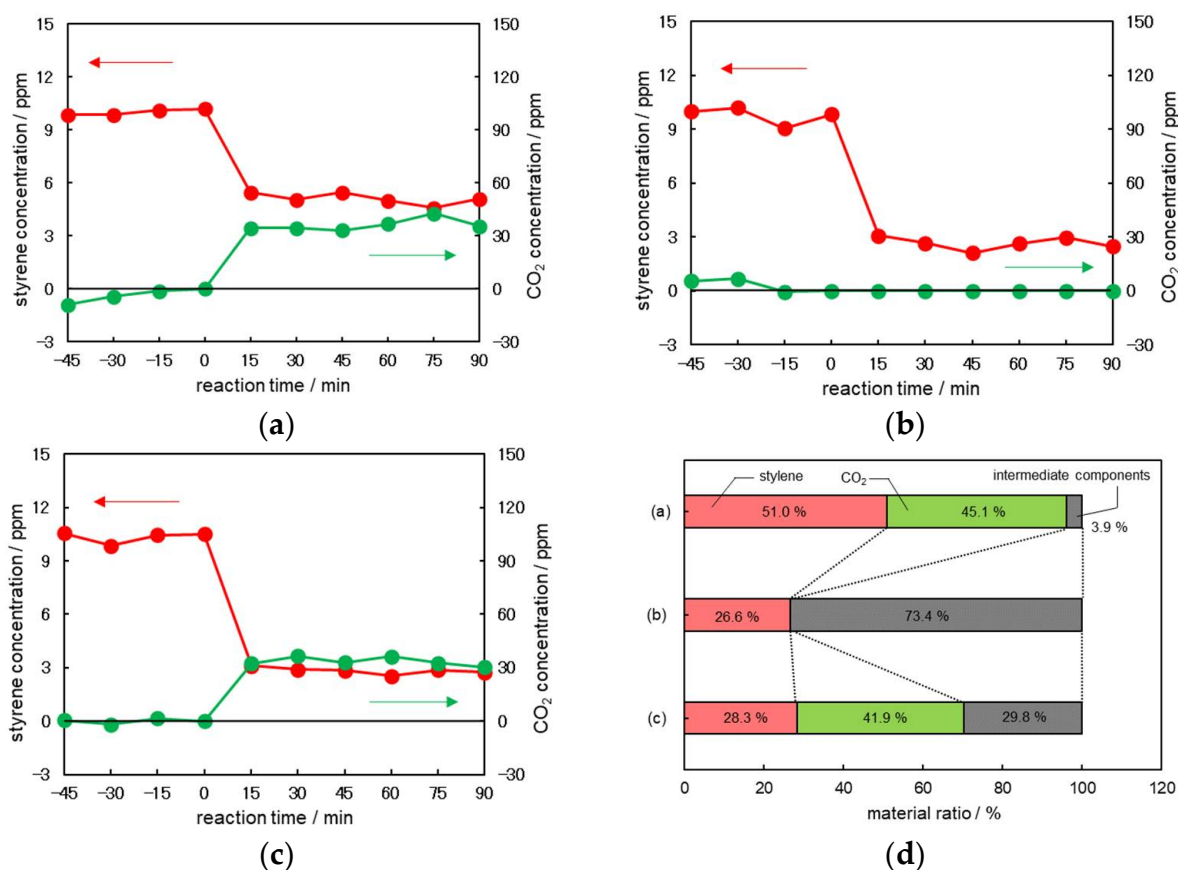

(**a**)

(**b**)

(**c**)

(**d**)

Figure 4. Typical data set of styrene removal (red) and CO_2 generation (green) by reaction with (**a**) photocatalyst + UV irradiation, (**b**) ozone + UV irradiation, (**c**) photocatalyst + ozone + UV irradiation, and (**d**) carbon material balance for each reaction (red: unreacted styrene components, green: generated CO_2 components, gray: generated intermediate components).

Figure 5 shows gas chromatograms of gas components (collected at the reactor outlet by activated carbon tube solvent extraction method) for each reaction (red: photocatalyst + UV irradiation, green: ozone + UV irradiation, blue: photocatalyst + ozone + UV irradiation). The chromatograms were normalized by the styrene peak (35.2 min). In the reaction of photocatalysis and UV irradiation, the oxide peaks shown in Figure 2 were not observed, and only styrene's peak appeared (red line). In the reaction of ozone and UV irradiation, the same peaks as in Figure 2 were observed, and they were estimated to be

benzene, benzaldehyde, and benzoic acid by similarity measures. Moreover, these peaks were also higher in intensity than the styrene peak (green line). In the reaction combining photocatalyst and ozone, peaks similar to those of the ozone-only reaction were identified, but the peaks of benzene, benzaldehyde, and benzoic acid were less intense than those of styrene (blue line).
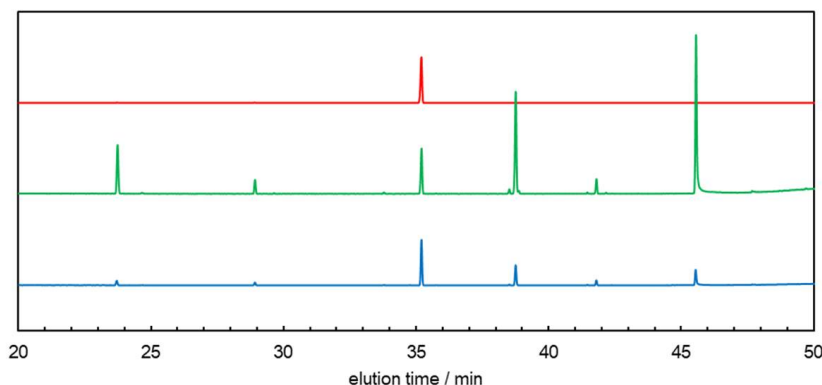

Figure 5. Gas chromatograms of gas components at reactor outlet by activated carbon tube solvent extraction method on each reaction (red: photocatalyst + UV irradiation, green: ozone + UV irradiation, blue: photocatalyst + ozone + UV irradiation).

Figure 6 shows residual ozone concentration (a) and residual rate of ozone (b) at the reactor outlet for each condition. For all ozone concentration conditions, ozone was not consumed without styrene in the reactor (black bars). When ozone and photocatalyst were combined, the ozone concentration at the reactor outlet decreased significantly. The remaining ozone was about 20–25% of the before reaction level, and thus less than half of that without the photocatalyst.
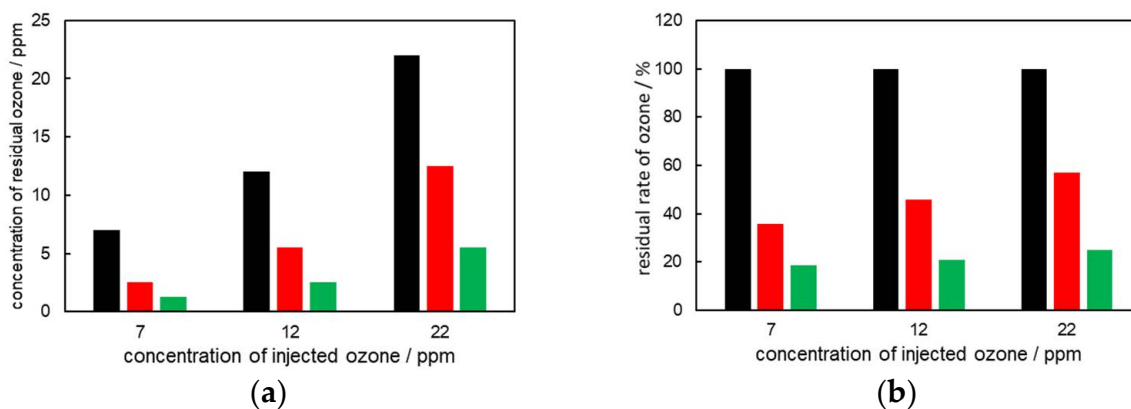

Figure 6. (**a**) Residual ozone concentration, (**b**) residual rate of ozone under each condition (black: without reaction, red: with ozone + UV irradiation, green: with photocatalyst + ozone + UV irradiation).

Figure 7 shows the relationship between the injected ozone concentration and residual styrene (red) and ozone (blue) concentrations on the decomposition of styrene using photocatalyst and ozone treatment. The styrene concentration in the reactor outlet gas decreased linearly with the injected ozone gas concentration. However, the ozone concentration increased linearly with the injected ozone gas concentration.
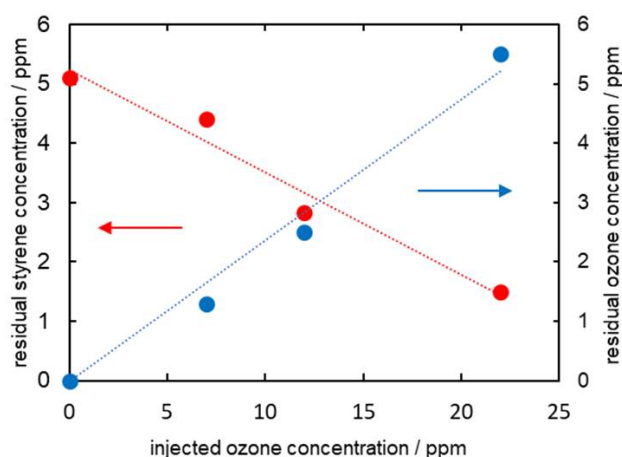
Figure 7. Relationship between injected ozone concentration and residual styrene (red), and ozone (blue) concentration on decomposition of styrene using photocatalyst and ozone treatment.

3. Discussion

Figures 1 and 3 show that the ozone injected into the reactor reacts with styrene gas and is consumed for the decomposition of styrene. It was also found that the styrene removal rate depended on the ozone concentration. Because the carbon dioxide concentration did not increase after the start of the reaction, this indicates that the ozone gas did not completely decompose styrene. In addition, the amount of styrene removed was constant regardless of UV irradiation, indicating that UV irradiation did not accelerate the decomposition process. Figure 2 shows that the gases released from the reactor outlet included benzene (23.8 min), styrene (35.2 min), benzaldehyde (38.8 min), styrene oxide (41.8 min), benzoic acid (45.6 min), and substances not recognized by the similarity measures (28.9 min). This suggests that ozone reacted with styrene and converted styrene into these compounds. In addition, carbon dioxide was not observed (Figure 1b), suggesting that the reaction was not a complete decomposition of the compounds observed in Figure 2. The chromatograms did not change with or without UV irradiation, and the positions of each peak and their intensity ratios did not change. This indicates that UV irradiation does not accelerate the decomposition process. Figure 3 shows that 50 to 70% of the ozone was consumed for the reaction with styrene, according to the amount of ozone injected. In addition, the ozone concentration decreased by approximately 5% with UV irradiation compared to that without irradiation. It is known that OH radicals are produced from ozone by UV irradiation [26,32–34]. Specifically, excited singlet oxygen is produced by UV irradiation of ozone below 310 nm, whereas excited triplet oxygen is produced by the visible light irradiation of ozone (>460 nm). OH radicals are generated from excited singlet oxygen [35]. Figure 8 shows the spectrum of the spot light used in the experiment and the absorption of ozone. Most of the UV light in the spot light is mainly concentrated in the 310–380 nm range, and there is insufficient light below 310 nm to produce excited singlet oxygen for the OH radicals. Therefore, it is considered that a spot light is suitable for the absorption of TiO_2, but not for the accelerated oxidation by ozone, and the production of OH radicals did not occur positively. The decrease in ozone concentration during UV irradiation observed in Figure 3 was due to the generation of active oxidative species such as OH radicals by a low intensity light below 310 nm, which did not drastically affect styrene removal. These results suggest that ozone is effective in oxidizing organic compounds to low molecular weight, but it is not sufficient for complete decomposition in a single pass; therefore, it is difficult to solve the air purification problem fundamentally by ozone gas treatment alone.
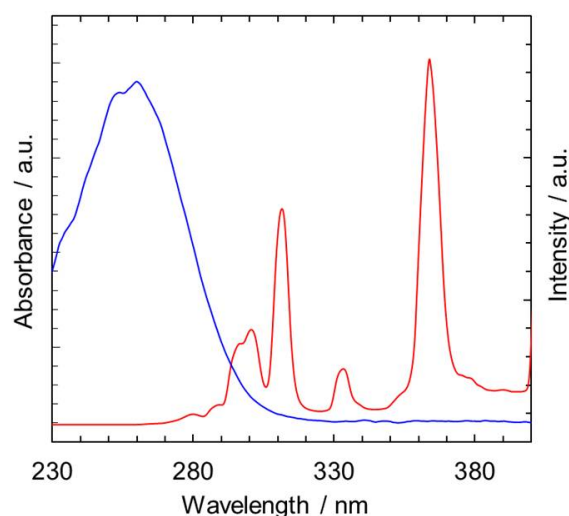
Figure 8. Spectrum of the spot light (red) and the ozone absorption curve (blue).

Figures 4 and 5 show the difference in the products of the photocatalytic reaction, the ozone reaction, and the reaction when these are combined. In the reaction of the photocatalyst only, 50% of the styrene was decomposed, and carbon dioxide was produced (Figure 4a,d). The amount of carbon dioxide produced was approximately 90% of the stoichiometry, suggesting that most of the styrene was decomposed into carbon dioxide. The reaction of ozone only shows higher styrene removal than the reaction of photocatalyst only, but no carbon dioxide production, indicating the production of intermediate products of benzene, benzaldehyde, and benzoic acid (Figure 4b,d and Figure 5). On the other hand, the reaction combining photocatalyst and ozone showed high styrene removal and carbon dioxide production (Figure 4c,d). The International Chemical Safety Cards (ICSCs) indicate that styrene and benzene are more toxic to humans than benzaldehyde and benzoic acid. Moreover, benzene, styrene, and styrene oxide are known to be carcinogenic [36,37]. Therefore, the trends of these compounds should be monitored carefully. The treatment combining photocatalyst and ozone removed about 70% of the styrene concentration. Benzene and styrene oxide showed very small peaks (23.8 min, 41.8 min) obtained by GCMS with solvent extraction (which can be estimated to be a concentration of ppb order or less). Therefore, it is assumed that the toxicity of the exhaust gas is reduced compared to the inlet gas. Moreover, it was found that the ozone concentration at the reactor outlet decreased after the photocatalyst was placed in the reactor (Figure 6). Therefore, it is suggested that ozone not only oxidizes styrene but also affects the photocatalyst surface.

The photocatalyst (TiO_2; p25) used in the experiment comprised nano-sized particles with a specific surface area of more than 50 m^2/g. Therefore, styrene and compounds produced by the reaction with ozone adsorb onto the photocatalyst surface. The adsorption of styrene and intermediate products in styrene decomposition on a photocatalyst has been previously reported [21,22]. In addition, extra ozone scavenges the radicals produced by the photocatalyst [38]. Therefore, we suggest that the decrease in ozone concentration is due to the attack of ozone on adsorbed compounds and consumption by radicals produced in the photocatalytic reaction. Figure 9 shows the proposed mechanisms of styrene decomposition using a photocatalyst and ozone treatment.

Figure 7 shows that it is possible to easily estimate the concentration of the exhausted odor components and the residual amount of ozone if the concentration of the inlet odor components is known in a one-pass reaction such as in an air purifier. When photocatalysts and ozone are combined in the air purifier, it is necessary to monitor the components exhausted from the air purifier, especially the ozone component, from the viewpoint of health. By monitoring the odor components in the atmospheric gas and applying the correct concentration of ozone gas to the photocatalytic reactor, the effect of ozone in the exhaust

gas on the human body can be suppressed as much as possible, and high-performance air purification can be achieved.
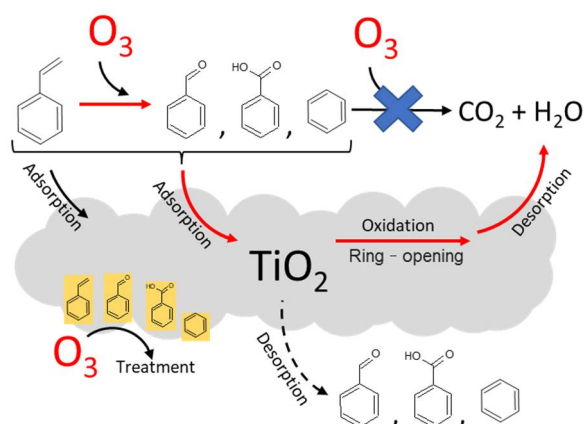

Figure 9. Proposed mechanisms of the decomposition of styrene using photocatalyst and ozone treatment.

4. Materials and Methods

A schematic of the experimental system is shown in Figure 10. In this study, styrene gas was prepared by the diffusion tube method using a permeator (PD-1 B, Gastec, INC., Tokyo, Japan). Dry air was supplied from a 7 m^3 compressed air cylinder (N$_2$: 80%, O$_2$: 20%), and humidified air was generated by bubbling dry air into a thermostatic glass bottle containing deionized water. The humidity of the test gas was adjusted by controlling the flow rate of dry air through the mass flow controller. Ozone gas was prepared by discharging air using an ozone generator (ED-OG-AP1, EcoDesign Inc., Saitama, Japan). The concentration of ozone gas was adjusted by controlling the flow rate of the air flowing into the ozone generator. Styrene gas, humidified air, and ozone gas were mixed and injected into a reactor (gas volume: 0.5 L, constructed of acrylic resin for the sides and bottom, and quartz glass for the top of the reactor). Furthermore, when ozone was not generated, air without discharge was mixed with styrene gas and humidified air instead of ozone gas. Therefore, the amount of styrene in the reactor remained constant, regardless of the reaction conditions. According to the method described above, the test gas injected into the reactor was controlled at 500 mL/min, 25 °C, and 50%RH (relative humidity). The photocatalyst powder (TiO$_2$ P 25, NIPPON AEROSIL, Tokyo, Japan) was spread evenly in a glass Petri dish (diameter: 6 cm) and placed in the center of the reactor. UV light (30 mW/cm^2, 310–380 nm, LA-310UV, Hayashi Clock Industry Co. Ltd., Tokyo, Japan) was emitted on the surface of the sample.
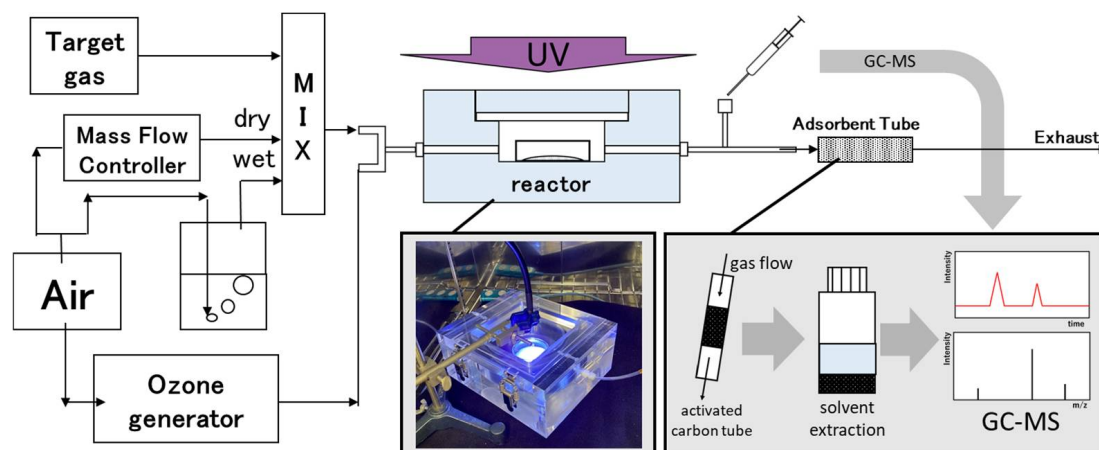

Figure 10. Photographs and schematic of evaluation equipment.

The gas at the reactor outlet was collected in activated carbon tubes (ORBO 101 Carbotrap, Supelco, Dorset, UK) for 30 min, and the adsorbent in the tubes was dipped in carbon disulfide for 5 min to extract the adsorbed components. The intermediate products at the reactor outlet were observed by GC-MS analysis using a GCMS-QP2010SE (Shimadzu, Kyoto, Japan), equipped with a DB-624 fused silica capillary column (60 m × 0.25 mm i.d. × 1.4 μm film, Agilent Technologies, Santa Clara, CA, USA). The initial oven temperature of 35 °C was held for 15 min and then raised to 240 °C over 35 min at a rate of 6 °C/min. The styrene concentration at the reactor outlet was measured by GC-MS analysis (GCMS-QP2010SE, Shimadzu, Kyoto, Japan). Carbon dioxide concentration at the reactor outlet was measured by GC analysis (GC-8A, Shimadzu, Kyoto, Japan), equipped with a 2 m Porapak-Q column, a methanizer, and a flame ionization detector, without heating the oven, and using N_2 as the carrier gas. The ozone concentration at the reactor outlet was measured using a gas detector tube system (Tube No. 182U and 182SB, Komyo Rikagaku Kogyo, Kanagawa, Japan).

5. Conclusions

In this study, we investigated the decomposition performance of ozone, a photocatalyst, and their combination on volatile organic compounds for application in indoor air purification. Using a one-pass mini reactor, the decomposition performance of each condition was evaluated by analyzing the outlet gas and observing the amount of styrene removed, the amount of carbon dioxide produced, and the composition of a small amount of intermediate products caused by the reaction. For further development into a practical application, among the three conditions tested, the combined condition of ozone and photocatalyst showed the highest air purification performance, with the ability of complete decomposition in the photocatalyst and the ability to remove odor components in ozone. Furthermore, we have successfully demonstrated that the decomposition performance of each condition could be evaluated and compared by observing slight amounts of intermediate products in the exhaust gas by GC-MS analysis, using the solvent extraction method. Previously, few studies have focused on the fundamental understanding of the decomposition of volatile organic compounds and the generation of intermediate products and standard methods of analysis for these technologies. In today's severely and diversely polluted indoor air, technologies for fundamentally decomposing odor compounds will be very useful for our society, and their engineering evaluation is an essential consideration; thus, we believe that the contribution of this research is significant. This study is expected to provide insights into the practical application of photocatalyst and ozone oxidation technologies in air purifiers and their performance management.

References

1. Fujishima, A.; Honda, K. Electrochemical Photolysis of Water at a Semiconductor Electrode. *Nature* **1972**, *238*, 37–38. [CrossRef] [PubMed]
2. Fujishima, A.; Rao, T.N.; Tryk, D.A. Titanium dioxide photocatalysis. *J. Photochem. Photobiol. Photochem. Rev.* **2000**, *1*, 1–21. [CrossRef]

3. Fujishima, A.; Zhang, X.; Tryk, D.A. TiO$_2$ photocatalysis and related surface phenomena. *Surf. Sci. Rep.* **2008**, *63*, 515–582. [CrossRef]

4. Hashimoto, K.; Irie, H.; Fujishima, A. TiO$_2$ Photocatalysis: A Historical Overview and Future Prospects. *Jpn. J. Appl. Phys.* **2005**, *44*, 8269–8285. [CrossRef]

5. Nakata, K.; Ochiai, T.; Murakami, T.; Fujishima, A. Photoenergy conversion with TiO$_2$ photocatalysis: New materials and recent applications. *Electrochim. Acta* **2012**, *84*, 103–111. [CrossRef]

6. Fujishima, A.; Zhang, X. Titanium dioxide photocatalysis: Present situation and future approaches. *C. R. Chim.* **2006**, *9*, 750–760. [CrossRef]

7. Ochiai, T.; Fujishima, A. Photoelectrochemical properties of TiO$_2$ photocatalyst and its applications for environmental purification. *J. Photochem. Photobiol. Photochem. Rev.* **2012**, *13*, 247–262. [CrossRef]

8. Ridley, M.K.; Hackley, V.A.; Machesky, M.L. Characterization and Surface-Reactivity of Nanocrystalline Anatase in Aqueous Solutions. *Langmuir* **2006**, *22*, 10972–10982. [CrossRef]

9. Luttrell, T.; Halpegamage, S.; Tao, J.; Kramer, A.; Sutter, E.; Batzill, M. Why is anatase a better photocatalyst than rutile?—Model studies on epitaxial TiO$_2$ films. *Sci. Rep.* **2014**, *4*, 4043. [CrossRef]

10. Buchalska, M.; Kobielusz, M.; Matuszek, A.; Pacia, M.; Wojtyła, S.; Macyk, W. On Oxygen Activation at Rutile- and Anatase-TiO$_2$. *ACS Catal.* **2015**, *5*, 7424–7431. [CrossRef]

11. Ochiai, T.; Hoshi, T.; Slimen, H.; Nakata, K.; Murakami, T.; Tatejima, H.; Koide, Y.; Houas, A.; Horie, T.; Morito, Y.; et al. Fabrication of TiO$_2$ Nanoparticles impregnated Titanium Mesh Filter and Its Application for Environmental Purification Unit. *Catal. Sci. Technol.* **2011**, *1*, 1324–1327. [CrossRef]

12. Chong, M.N.; Jin, B.; Chow, C.W.K.; Saint, C. Recent developments in photocatalytic water treatment technology: A review. *Water Res.* **2010**, *44*, 2997–3027. [CrossRef] [PubMed]

13. Shayegan, Z.; Lee, C.-S.; Haghighat, F. TiO$_2$ photocatalyst for removal of volatile organic compounds in gas phase—A review. *Chem. Eng. J.* **2018**, *334*, 2408–2439. [CrossRef]

14. Ochiai, T.; Aoki, D.; Saito, H.; Akutsu, Y.; Nagata, M. Analysis of Adsorption and Decomposition of Odour and Tar Components in Tobacco Smoke on Non-Woven Fabric-Supported Photocatalysts. *Catalysts* **2020**, *10*, 304. [CrossRef]

15. Matsuura, R.; Lo, C.-W.; Wada, S.; Somei, J.; Ochiai, H.; Murakami, T.; Saito, N.; Ogawa, T.; Shinjo, A.; Benno, Y.; et al. SARS-CoV-2 Disinfection of Air and Surface Contamination by TiO$_2$ Photocatalyst-Mediated Damage to Viral Morphology, RNA, and Protein. *Viruses* **2021**, *13*, 942. [CrossRef] [PubMed]

16. Ito, T.; Sunada, K.; Nagai, T.; Ishiguro, H.; Nakano, R.; Suzuki, Y.; Nakano, A.; Yano, H.; Isobe, T.; Matsushita, S.; et al. Preparation of cerium molybdates and their antiviral activity against bacteriophage Φ6 and SARS-CoV-2. *Mater. Lett.* **2021**, *290*, 129510. [CrossRef]

17. Slimen, H.; Ochiai, T.; Nakata, K.; Murakami, T.; Houas, A.; Morito, Y.; Fujishima, A. Photocatalytic Decomposition of Cigarette Smoke Using a TiO$_2$-Impregnated Titanium Mesh Filter. *Ind. Eng. Chem. Res.* **2012**, *51*, 587–590. [CrossRef]

18. *JIS R 1701-2:2016*; Fine Ceramics (Advanced Ceramics, Advanced Technical Ceramics)—Test Method for Air Purification Performance of Photocatalytic Materials—Part 2: Removal of Acetaldehyde. Japanese Standards Association: Tokyo, Japan, 2016.

19. *ISO 22197-2:2011*; Fine Ceramics, Advanced Technical Ceramics—Test Method for Air-Purification Performance of Semiconducting Photocatalytic Materials—Part 2: Removal of Acetaldehyde. ISO/TC 206 Japan Fine Ceramics Association: Tokyo, Japan, 2011.

20. Ohko, Y.; Tryk, D.A.; Hashimoto, K.; Fujishima, A. Autoxidation of Acetaldehyde Initiated by TiO$_2$ Photocatalysis under Weak UV Illumination. *J. Phys. Chem.* **1998**, *102*, 2699–2704. [CrossRef]

21. Chen, J.; He, Z.; Ji, Y.; Li, G.; An, T.; Choi, W. OH radicals determined photocatalytic degradation mechanisms of gaseous styrene in TiO$_2$ system under 254 nm versus 185 nm irradiation: Combined experimental and theoretical studies. *Appl. Catal. Environ.* **2019**, *257*, 117912. [CrossRef]

22. Zhang, W.; Li, G.; Liu, H.; Chen, J.; Ma, S.; Wen, M.; Kong, J.; An, T. Photocatalytic degradation mechanism of gaseous styrene over Au/TiO$_2$@CNTs: Relevance of superficial state with deactivation mechanism. *Appl. Catal. Environ.* **2020**, *272*, 118969. [CrossRef]

23. Nagayoshi, M.; Kitamura, C.; Fukuizumi, T.; Nishihara, T.; Terashita, M. Antimicrobial Effect of Ozonated Water on Bacteria Invading Dentinal Tubules. *J. Endod.* **2004**, *30*, 778–781. [CrossRef] [PubMed]

24. Ochiai, T.; Tago, S.; Hayashi, M.; Hirota, K.; Kondo, T.; Satomura, K.; Fujishima, A. Boron-doped diamond powder (BDDP)-based polymer composites for dental treatment using flexible pinpoint electrolysis unit. *Electrochem. Commun.* **2016**, *68*, 49–53. [CrossRef]

25. Gervasini, A.; Vezzoli, G.C.; Ragaini, V. VOC removal by synergic effect of combustion catalyst and ozone. *Catal. Today* **1996**, *29*, 449–455. [CrossRef]

26. Hamada, K.; Ochiai, T.; Tsuchida, Y.; Miyano, K.; Ishikawa, Y.; Nagura, T.; Kimura, N. Eco-Friendly Cotton/Linen Fabric Treatment Using Aqueous Ozone and Ultraviolet Photolysis. *Catalysts* **2020**, *10*, 1265. [CrossRef]

27. Shen, Y.-S.; Ku, Y. Treatment of gas-phase volatile organic compounds (VOCs) by the UVO3 process. *Chemosphere* **1999**, *38*, 1855–1866. [CrossRef]

28. Tripathi, S.; Hussain, T. Chapter 7—Water and Wastewater Treatment through Ozone-based technologies. In *Development in Wastewater Treatment Research and Processes*; Shah, M., Rodriguez-Couto, S., Biswas, J., Eds.; Elsevier: Amsterdam, The Netherlands, 2022; pp. 139–172.

29. Ochiai, T.; Nakata, K.; Murakami, T.; Morito, Y.; Hosokawa, S.; Fujishima, A. Development of an Air-Purification Unit Using a Photocatalysis-Plasma Hybrid Reactor. *Electrochemistry* **2011**, *79*, 838–841. [CrossRef]

30. Mills, A.; Lee, S.-K.; Lepre, A. Photodecomposition of ozone sensitised by a film of titanium dioxide on glass. *J. Photochem. Photobiol. Chem.* **2003**, *155*, 199–205. [CrossRef]

31. Sánchez, L.; Peral, J.; Domènech, X. Aniline degradation by combined photocatalysis and ozonation. *Appl. Catal. Environ.* **1998**, *19*, 59–65. [CrossRef]

32. Sharma, V.K.; Graham, N.J.D. Oxidation of Amino Acids, Peptides and Proteins by Ozone: A Review. *Ozone Sci. Eng.* **2010**, *32*, 81–90. [CrossRef]

33. Ikehata, K.; Jodeiri Naghashkar, N.; Gamal El-Din, M. Degradation of Aqueous Pharmaceuticals by Ozonation and Advanced Oxidation Processes: A Review. *Ozone Sci. Eng.* **2006**, *28*, 353–414. [CrossRef]

34. Panda, S.K.B.C.; Sen, K.; Mukhopadhyay, S. Sustainable pretreatments in textile wet processing. *J. Clean. Prod.* **2021**, *329*, 129725. [CrossRef]

35. Matsumi, Y.; Comes, F.J.; Hancock, G.; Hofzumahaus, A.; Hynes, A.J.; Kawasaki, M.; Ravishankara, A.R. Quantum yields for production of $O(^1D)$ in the ultraviolet photolysis of ozone: Recommendation based on evaluation of laboratory data. *J. Geophys. Res. Atmos.* **2002**, *107*, ACH-1. [CrossRef]

36. Lai, H.K.; Jantunen, M.J.; Künzli, N.; Kulinskaya, E.; Colvile, R.; Nieuwenhuijsen, M.J. Determinants of indoor benzene in Europe. *Atmos. Environ.* **2007**, *41*, 9128–9135. [CrossRef]

37. Phillips, D.H.; Farmer, P.B. Evidence for DNA and Protein Binding by Styrene and Styrene Oxide. *Crit. Rev. Toxicol.* **1994**, *24*, S35–S46. [CrossRef]

38. Zhang, P.; Liu, J. Photocatalytic degradation of trace hexane in the gas phase with and without ozone addition: Kinetic study. *J. Photochem. Photobiol. Chem.* **2004**, *167*, 87–94. [CrossRef]